



# High-frequent pulsing ablation of C/C–SiC–ZrB<sub>2</sub>–ZrC composite for different cycles to 2000 times in plasma

Wei FENG<sup>1</sup>, Yan ZHANG<sup>1</sup>, Lei LIU<sup>1</sup>, Bo-yan LI<sup>1</sup>, Jia-ping ZHANG<sup>2</sup>,  
Xi CHEN<sup>3</sup>, Zi-bo HE<sup>1</sup>, Cheng-wei TANG<sup>1</sup>, Hai-jun ZHANG<sup>1</sup>, Qin-xin HAN<sup>1</sup>

1. School of Materials and Chemical Engineering, Xi'an Technological University, Xi'an 710021, China;
2. State Key Laboratory of Solidification Processing, Northwestern Polytechnical University, Xi'an 710072, China;
3. Xi'an Rare Metal Materials Institute Co., Ltd., Xi'an 710072, China

Received 29 September 2021; accepted 12 January 2022

**Abstract:** The high-frequent pulsing ablation of C/C–SiC–ZrB<sub>2</sub>–ZrC composites under millisecond-scaled single loading for different cycles was studied. The sample was ablated and cooled by plasma and airflow alternately on a self-developed bench. Results indicated that the ablation rates decreased quickly before 1000 cycles and then declined gradually until impact for 2000 cycles. Microstructure, phase and surface temperature analyses suggested that an incomplete layer of mixed ceramic ablation product was formed on the surfaces of the tested composites and the amount of the bare carbon tended to be steady after 1000 cycles. The ablation product layer weakened the thermal stress-induced mechanical erosion and protected the carbon from erosion, which led to the evolution of ablation rates.

**Key words:** cyclic ablation; pulsing ablation; C/C composite; SiC–ZrB<sub>2</sub>–ZrC; cycles

## 1 Introduction

C/C composites possess many good properties such as low density and coefficient of thermal expansion, high specific strength, outstanding anti-wear ability, superior thermal shock and ablation resistance [1–5]. The composites have been used as nozzle of solid rocket engine, thermal protective system of high speed aircraft, brake disks of aircraft and racing cars, and so on [6–10]. After continuous modification for several decades, the cost of the composites is reduced and the properties are greatly improved. Up to now, the advanced C/C composites are not only the competitive materials for nozzle of repetitive starting liquid rocket engine, but also potential materials for future piston of high power density diesel engine and pantographic slipper of high speed railway [11,12]. When used as

the above components, combustion at ultra-high temperature will attack the composites periodically. The single loading time is as short as millisecond scale and the frequency could be a few tenths to dozens of Hertz [13,14]. The working condition is markedly different from the continuous loading environment, and also happened for the barrel of quick-firing gun [15] and electric brush [16].

Some work has been done to understand the cyclic ablation of various C/C composites [17–30]. It has been found that chemical composition [31], interface [32] and microstructure [33] of C/C composites were important to the cyclic ablation behavior. Furthermore, the loading method like single impacting time was also significant to the cyclic ablation characteristics [34,35]. However, the single impacting time varies from several to hundreds of seconds while the millisecond-scaled single loading was rarely reported [36], and the

**Corresponding author:** Lei LIU, Tel: +86-13629209053, E-mail: [liuleiNIN@126.com](mailto:liuleiNIN@126.com);

Xi CHEN, Tel: +86-15229002899, E-mail: [chenxb@nwpu.edu.cn](mailto:chenxb@nwpu.edu.cn)

DOI: 10.1016/S1003-6326(22)66127-2

1003-6326/© 2023 The Nonferrous Metals Society of China. Published by Elsevier Ltd & Science Press

cyclic ablation in most of the research was no more than 20 cycles [37]. In our recent work [36], it has been found that the ablation rates of C/C–SiC–ZrB<sub>2</sub>–ZrC composites under millisecond-scaled single loading were much lower than those for longer time whereas the evolution of the cyclic ablation with loading cycles is still unknown.

To the piston and pantographic slipper, 2000 times thermal impacting has been widely used to evaluate the feasibility of the material before component and bench tests. And the evolution of tested material varying with loading times is important for the reliability assessment and material optimizing. Thus, C/C–SiC–ZrB<sub>2</sub>–ZrC composite possessing good anti-oxidation ability in a wide temperature range [38–40] was ablated and cooled by alternant plasma and airflow for different cycles to 2000 times at millisecond-scaled single loading to understand the ablation behavior and mechanism in the present work.

## 2 Experimental

C/C–SiC–ZrB<sub>2</sub>–ZrC composite was fabricated through infiltration of pyrocarbon (PyC), then

ZrB<sub>2</sub>–ZrC and finally SiC. 2.5D needle-punched carbon fiber felt with density of 0.4–0.5 g/cm<sup>3</sup> was used as the reinforcement. The pyrocarbon matrix was prepared by thermal gradient chemical vapor infiltration with methane as carbon source at 1225–1423 K. ZrB<sub>2</sub>–ZrC and SiC matrices were introduced into the porous C/C skeleton through precursor infiltration and pyrolysis. The pyrolysis was performed in a flowing Ar atmosphere at 1673–2073 K for 2 h. Other details of the preparation could be found in our previous papers [34,41]. The bulk density of the prepared composite was 2.0 g/cm<sup>3</sup> with 50.02 wt.% ceramics (mass ratio of SiC-to-ZrB<sub>2</sub>-to-ZrC was 2:1:2).

Disk samples ( $d30\text{ mm} \times 10\text{ mm}$ ) were ablated on a self-developed bench depended on a plasma generator (Multiplaz 3500) and compressed air. As shown in Fig. 1(a), the C/C–SiC–ZrB<sub>2</sub>–ZrC sample was ablated and cooled by plasma and airflow alternately. Single loading time of both the plasma and airflow was 0.2 s and time of the movement between these two fluids was 0.4 s. The temperature of the impacted plasma was about 2600 K which was ascertained by a porous zirconia. Detailed parameters of the ablation test are given in Table 1.

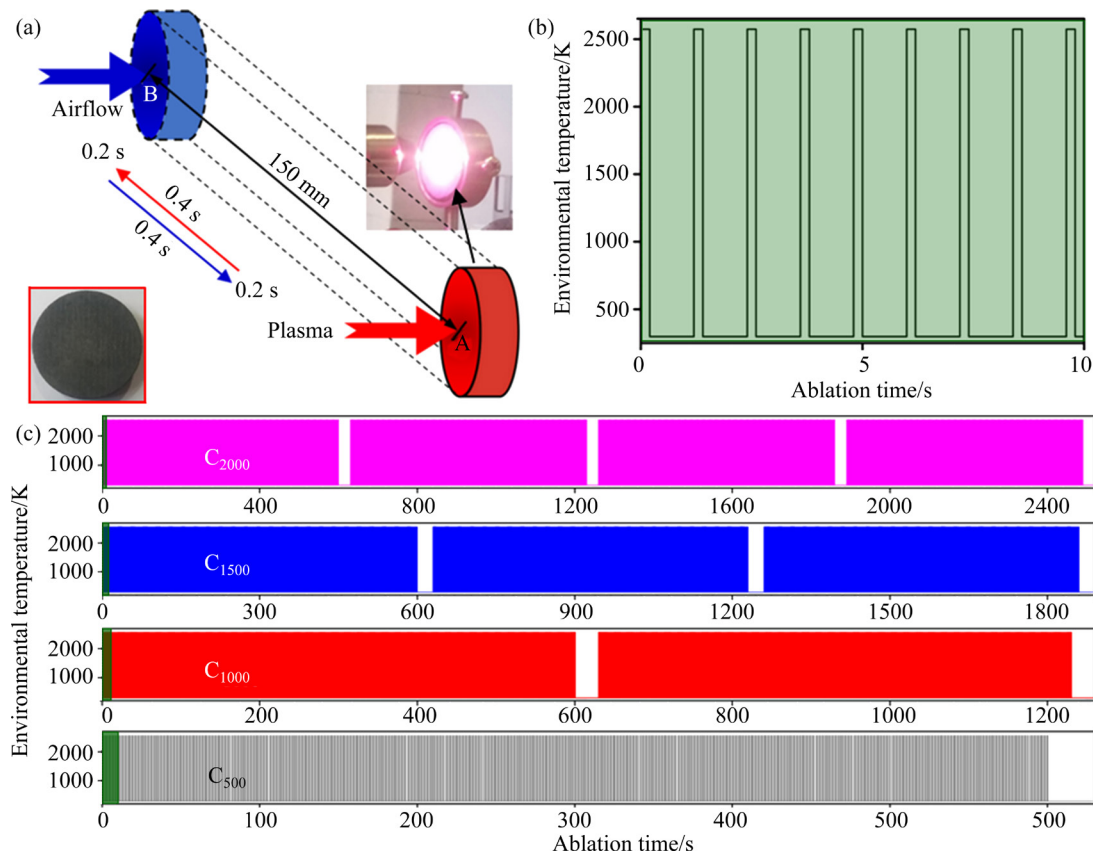


**Fig. 1** Schematic diagrams of ablation test (a), impacting method (b) and loading spectra (c) of tested samples

**Table 1** Parameters of high-frequent pulsing ablation test

Parameter	Value
Voltage of plasma/V	160
Current of plasma/A	6
Pressure of airflow/MPa	0.4
Flux of airflow/(m <sup>3</sup> ·h <sup>-1</sup> )	2
Temperature of plasma/K	2600
Temperature of airflow/K	RT
Single loading time/s	0.2
Impacting angle/(°)	90
Distance from gun tip to sample surface/mm	10
Inner diameter of gun tip/mm	2
Distance between plasma and airflow/mm	150
Period of every cycle/s	1.2
Cycles for every start–stop	500

The cyclic ablation test was carried out according to the loading spectra shown in Figs. 1(b, c). All the green areas of the four spectra in Fig. 1(c) corresponded to the loading cycles at the first 10 s shown in Fig. 1(b). By adjusting the times of start–stop, four kinds of ablation cycles of C500, C1000, C1500 and C2000 were achieved. During ablation, surface temperature of the tested sample was monitored by an infrared thermometers of Endurance E3ML (323–1273 K with precision of  $\pm 0.3\%$ , and response time of 20 ms). The ablation rates were calculated according to the changes of the whole mass and surface central thickness before and after ablation.

The phase, micro-morphology and chemical ingredient of the composites before and after ablation were characterized by an X-ray diffraction (XRD, X'Pert Pro MPD) and a scanning electron microscopy (SEM, JSM6460) combined with energy dispersive spectroscopy (EDS).

### 3 Results and discussion

Figures 2 and 3 show the microstructure and XRD pattern of the prepared C/C–SiC–ZrB<sub>2</sub>–ZrC composite. It can be seen that the composite was composed of C, SiC and ZrB<sub>2</sub>–ZrC. The lamellar structure of the composite was clear in the cross-sectional morphology (Fig. 2(a)). Figure 2(b) displays that the PyC coated carbon fibers were further wrapped by ZrB<sub>2</sub>–ZrC particles, and the granular SiC situated at the residual pores. Moreover, the needle-punched zone (marked by C

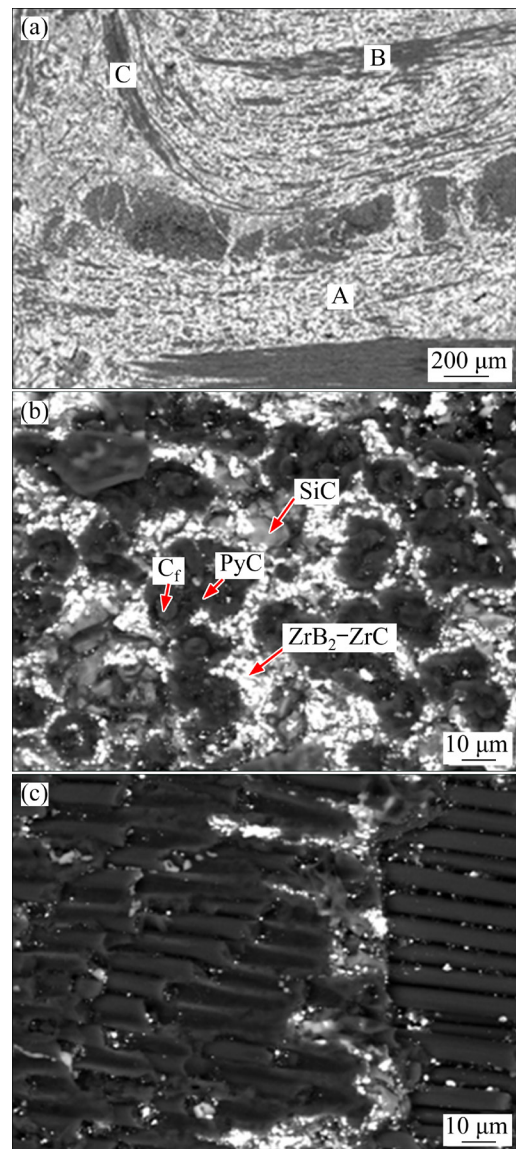


**Fig. 2** Microstructures of prepared C/C–SiC–ZrB<sub>2</sub>–ZrC composite: (a) At low magnification; (b) Magnified A zone; (c) Magnified B zone

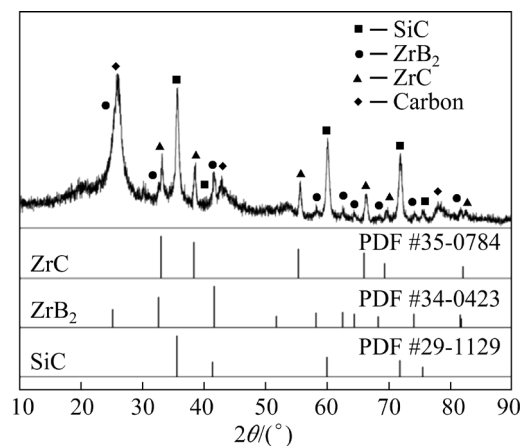


**Fig. 3** XRD pattern of prepared C/C–SiC–ZrB<sub>2</sub>–ZrC composite

in Fig. 2(a)) was similar to the non-woven layer (marked by B in Fig. 2(a)). And the further magnified morphology of B zone indicated that both  $ZrB_2$ -ZrC and SiC filled into the inner pores of fiber bundles in non-woven layer.

Figure 4 shows the ablation rates and the ablated macro-morphologies of the C/C-SiC-ZrB<sub>2</sub>-ZrC composite according to different loading spectra of Fig. 1(c). With rising of impact cycles of plasma, the ablation rates decreased quickly before 1000 cycles and then declined gradually until up to 2000 cycles. The evolution of the ablation rates

suggested that the surface anti-ablation ability was enhanced with increasing ablation cycles. By comparing the ablated macro-morphologies with those before ablation (image at the bottom left corner of Fig. 1(a)), it could be found that some white phases were formed on the surface. This might be the reason of the decreased ablation rates.

The surface central backscattered electron morphologies of the ablated C/C-SiC-ZrB<sub>2</sub>-ZrC composites according to different loading spectra of Fig. 1(c) are shown in Fig. 5. In comparison with the morphology before ablation (Fig. 2(a)), it could

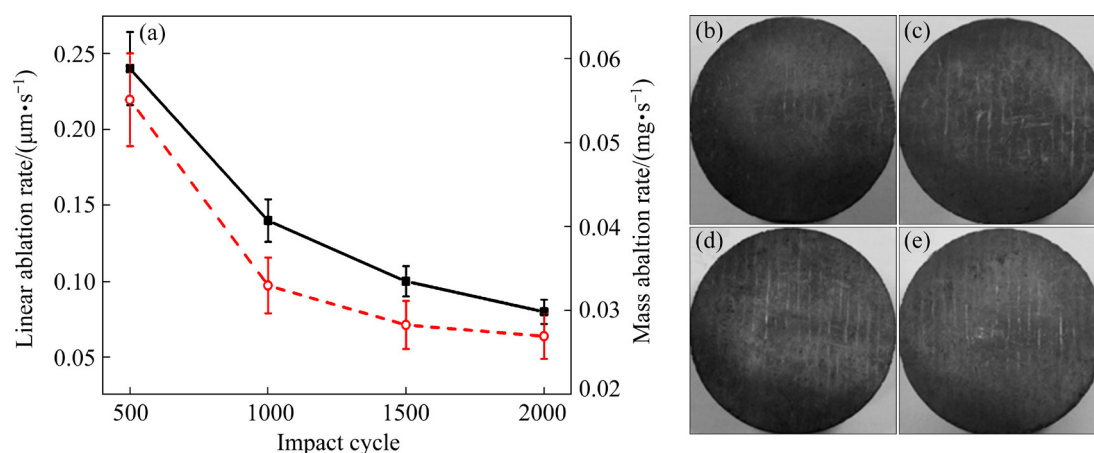


**Fig. 4** Ablation rates (a) and macro-morphologies (b–e) of ablated C/C-SiC-ZrB<sub>2</sub>-ZrC samples according to spectra of C<sub>500</sub> (b), C<sub>1000</sub> (c), C<sub>1500</sub> (d) and C<sub>2000</sub> (e)

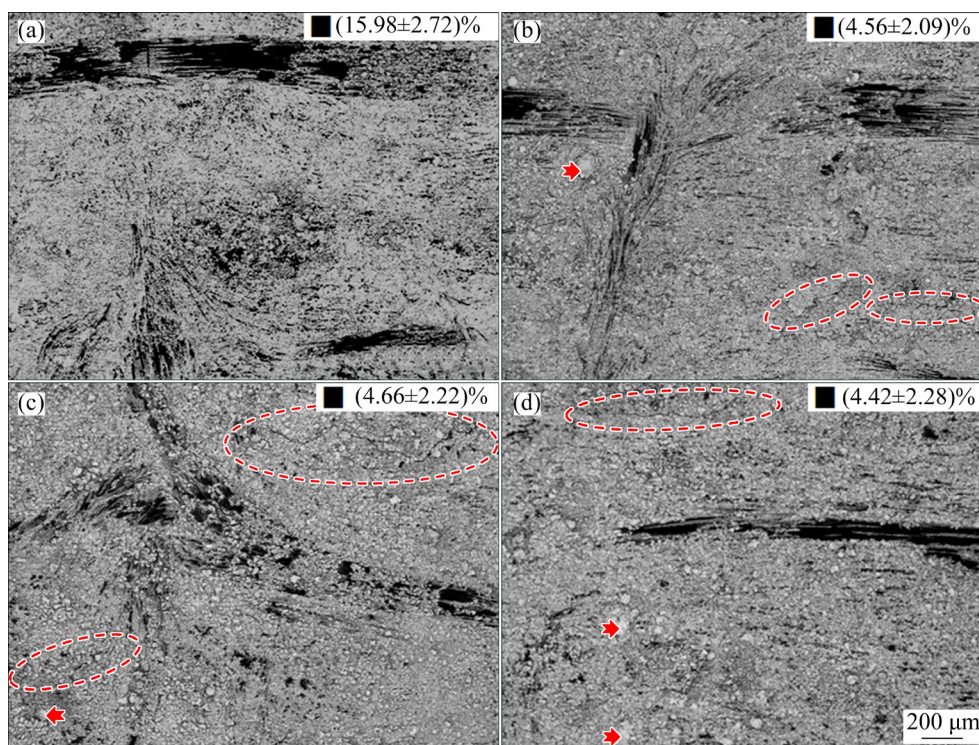


**Fig. 5** Surface central morphologies of ablated C/C-SiC-ZrB<sub>2</sub>-ZrC samples at low magnification according to spectra of C<sub>500</sub> (a), C<sub>1000</sub> (b), C<sub>1500</sub> (c) and C<sub>2000</sub> (d) (Insert at the top right corner: Corresponding proportion of black area calculated by Image J)

be seen that most of the black carbon was covered by some white phase. Moreover, the amount of bare carbon (presented at the top right corner of corresponding figure) became steady after 1000 pulsing cycles of plasma, which was related to the evolution of ablation rates. As marked by the red ellipse of dash line, some micro-cracks located at the ceramic rich region. And the diameters of the sintered particles which were marked by red arrows kept stable with rising ablation cycles. Thus, it could be inferred that some of the ablation product layers were peeled off persistently during the high frequent cyclic ablation test. As a result, the slightly fluctuated amount of the bare carbon from 1000 to 2000 cycles was reasonable as the ablation came into dynamic equilibrium after 1000 cycles.

Figure 6 shows surface central morphologies and relevant EDS analysis results of the web layers of the ablated C/C–SiC–ZrB<sub>2</sub>–ZrC composite according to different loading spectra of Fig. 1(c). There were two kinds of Si–Zr–B–O phases on the surface, and both phases were partially oxidized ceramics depending on the stoichiometric ratio. The cumulus white Si-poor phase was compact and presented a sintering state, whereas the gray Si-rich phase was rimous. The Si-rich phase should be the sub layer or out layer [42,43] of the Si-poor phase

under continuous impacting of combustion, which further demonstrated that the surface particles were peeled off during the high frequent pulsing cyclic ablation. Besides, the broken fibers (marked by arrow in Fig. 7) on the ablated surface centers of the non-woven layers suggested that mechanical erosion acted as a key role in the ablation.

XRD patterns of the ablated C/C–SiC–ZrB<sub>2</sub>–ZrC composite are displayed in Fig. 8. The diffraction peaks of carbon were greatly weakened whereas the peaks of ceramics became stronger after ablation. And all the ZrC disappeared while ZrO<sub>2</sub> came into being, which indicated that ZrC was oxidized during ablation. However, ZrB<sub>2</sub> should have a priority to be oxidized than others in the oxidizing environment depending on the thermodynamics [30]. Reconsidering the mixed state of ZrB<sub>2</sub>–ZrC and the stoichiometric ratio of Si–Zr–B–O phases in Fig. 6, it could be inferred that the oxidation of ZrB<sub>2</sub> might be inhibited by B<sub>2</sub>O<sub>3</sub>. Moreover, comparison of the relative intensities (marked by the arrows) between ZrB<sub>2</sub> and ZrO<sub>2</sub> peaks suggested that the content of ZrO<sub>2</sub> changed with increasing ablation cycles but no trend could be observed, which signified that the ZrO<sub>2</sub> was formed and consumed simultaneously. This phenomenon was in accordance with the analysis of

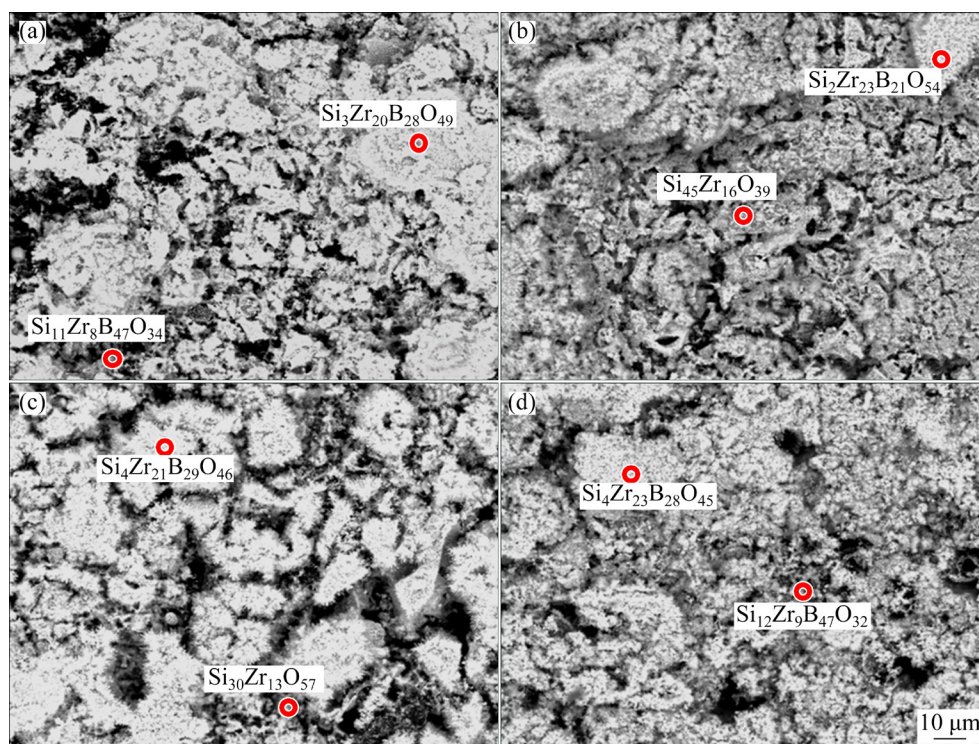


**Fig. 6** Surface central morphologies of web layer of ablated C/C–SiC–ZrB<sub>2</sub>–ZrC samples and relevant EDS analysis results according to spectra of C<sub>500</sub> (a), C<sub>1000</sub> (b), C<sub>1500</sub> (c) and C<sub>2000</sub> (d)

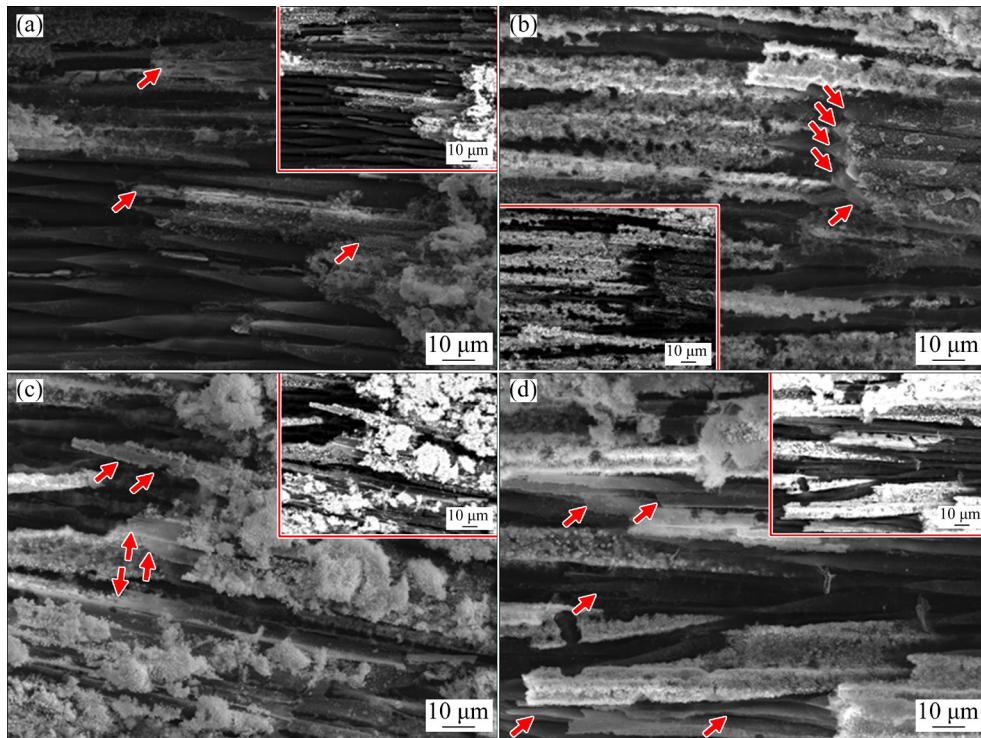


**Fig. 7** Surface central morphologies of non-woven layer of ablated C/C–SiC–ZrB<sub>2</sub>–ZrC samples according to spectra of C<sub>500</sub> (a), C<sub>1000</sub> (b), C<sub>1500</sub> (c) and C<sub>2000</sub> (d) (Insert figure at the corner: Relevant backscattered electron image)

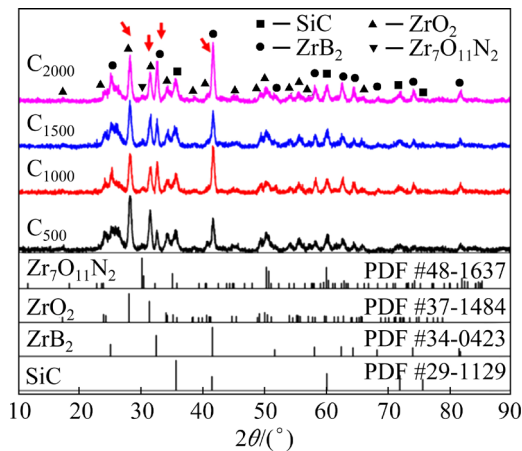


**Fig. 8** XRD patterns of ablated C/C–SiC–ZrB<sub>2</sub>–ZrC samples

the ablated morphologies. Besides, the missing diffraction peaks of possibly existing B<sub>2</sub>O<sub>3</sub> and SiO<sub>2</sub> might be caused by the few amount or the fast cooling induced amorphous states.

Figure 9 shows the surface temperatures of the C/C–SiC–ZrB<sub>2</sub>–ZrC samples during ablation. It was notable that the surface temperature of the sample was much lower than that of the plasma. According to the heat transfer theory, the surface temperature tended to be as same as that of the plasma with the loading time extended. However,

the single loading time was 0.2 s, which was too short to result in a high surface temperature. Besides, the heated surface was cooled by airflow at the impacting interval of the plasma. Thus, the surface temperature stabilized at about 600 K after certain loading cycles. Corresponding to the impacting method and loading spectra in Fig. 1, the surface temperatures fluctuated with the loading–unloading and start–stop cycles. The peak and amplitude of the surface temperature kept relatively stable but still waved all the time, which indicated that the composition and phases of the ablated surface was in dynamic state through the whole cyclic ablation. This was because the measured temperature reflected surface radiant characteristics depending on the principle of infrared temperature measurement. Moreover, marked by the two-way arrows (Fig. 9), it was clear that the duration of unsteady fluctuation at the beginning became shorter with the increasing of start–stop cycle. Both the above temperature evolutions should be caused by the accumulation and peeling-off of ablation products. Furthermore, the surface temperature was lower than 600 K all the time. It was confusing that how the cyclic ablation worked in such a low temperature which was below the starting oxidation

temperatures of all the components of the composite.

To understand the high-frequent pulsing ablation mechanism under different loading cycles,

a schematic diagram is shown in Fig. 10. The wave in box which was displayed in the figure represented the infrared ray from the ablated sample and its amount indicated the infrared intensity.

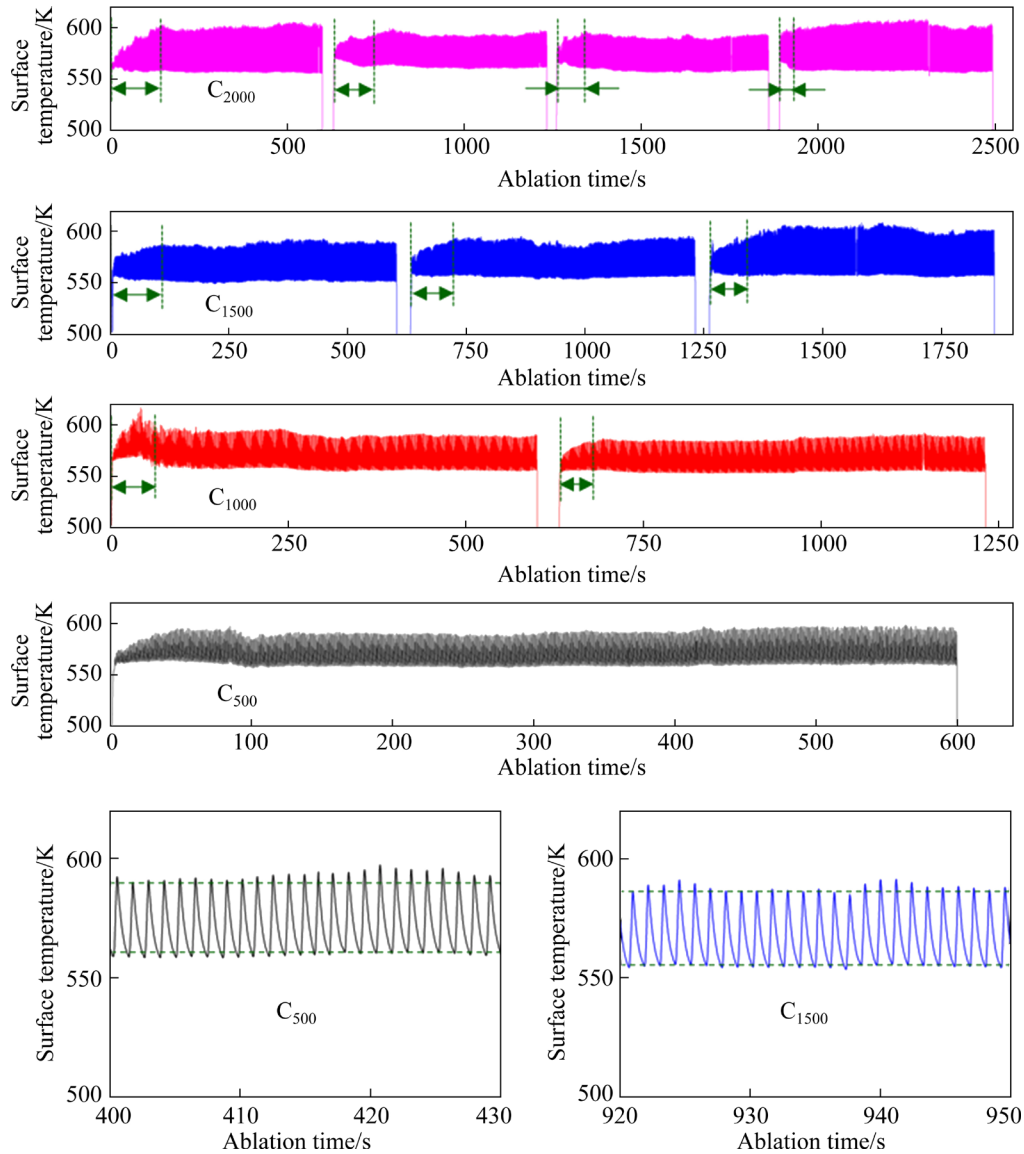


Fig. 9 Surface temperatures of C/C-SiC-ZrB<sub>2</sub>-ZrC samples during ablation

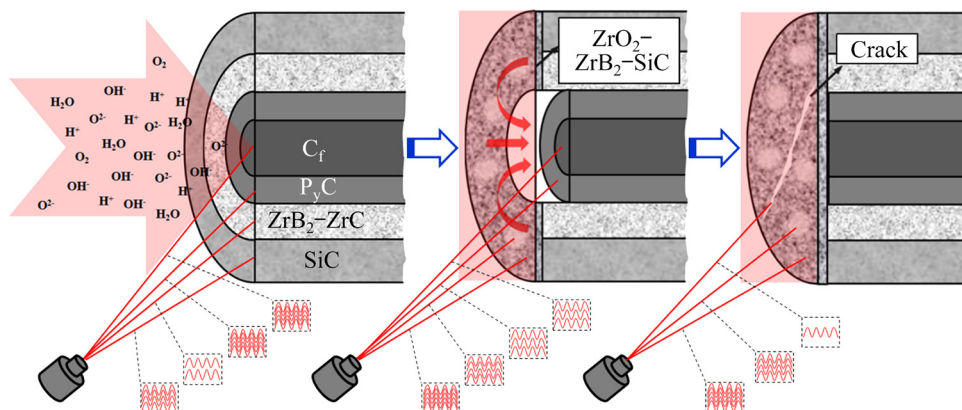


Fig. 10 Schematic diagrams of high-frequency pulsing ablation mechanism

More waves suggested stronger infrared intensity, which was on behalf of the higher temperature. When plasma was impacted on the original surface of the C/C–SiC–ZrB<sub>2</sub>–ZrC sample, the composite would be heated to higher temperature by the ionized H<sub>2</sub>O and mixed air. The diverse zones of the composite obtained different quantities of heat due to their various emissivity as thermal radiation dominated the heat exchange [36,44]. Thus, the carbon and SiC phases acted as the hot points which had higher temperature than the ZrB<sub>2</sub>–ZrC. And more infrared radiation messages at certain wavelengths from carbon and SiC were detected by the thermometer. In another word, the temperature of carbon and SiC was higher than the measured average value. Therefore, oxidation could happen at these hot points. Meanwhile, some carbon fibers were broken by thermal stress, as shown in Fig. 7(a). With consumption of the carbon through oxidation and shear fracture, the nearby partially-oxidized ZrB<sub>2</sub>–ZrC and SiC spread out under shearing force of the combustion flow and covered the sunk carbon. At the same time, these ceramic particles sintered as their oxidation elevated the emissivity and some oxides acted as the aids. This process was similar to the fabrication of materials under spark plasma sintering. Finally, the surface was coated by the mixed ceramics while some cracks appeared under the high-frequent alternate loading of combustion and airflow.

Obviously, the oxidation was feasible in the view of thermodynamics, but just played a limited role in ablation since the single heating time was too short and was accompanied by following air-cooling. Besides the low surface temperature, when taking all the micro-cracks located at the ceramic-rich region and stable sizes of the sintered particles (Fig. 5), broken fibers (Fig. 7), fluctuated ZrO<sub>2</sub> peaks (Fig. 8) and waved peak and amplitude of surface temperature (Fig. 9) into consideration, it could be inferred that mechanical erosion dominated the ablation while thermal chemical erosion and phase transition acted as the assistant factors. The transient impacting of plasma and cooling airflow would lead to three kinds of mechanical erosions: (1) one was caused by temperature difference between inside and outside, (2) another one was determined by various surface phases, and (3) the last one was resulted from the scour of fluid. With accumulation of the ablation

products, the former two mechanical erosions were weakened as the surface carbon was covered by ceramics containing large amount of ZrO<sub>2</sub>. The heat was insulated by the surface ablation products and the thermal physical differences between the two mixed ceramics of Si–Zr–B–O phases were smaller than those of the original surface phases. Meanwhile, the oxidations of the carbon fiber and matrix were also protected by the ablation product. Furthermore, the mixed ceramic phases, especially for the sintered compact Si-poor phase, could not survive from the peeling-off of combustion flow under the high-frequent severe thermal shock. As a result, the ablation rates decreased quickly first and then declined gradually.

## 4 Conclusions

(1) When ablated under millisecond-scaled single loading at high frequency, the ablation rates of C/C–SiC–ZrB<sub>2</sub>–ZrC composites decreased quickly before 1000 cycles and then declined gradually until impact for 2000 cycles.

(2) An incomplete layer of mixed ceramic ablation product was formed on the surfaces of the tested composites and the amount of the bare carbon tended to be steady after 1000 cycles.

(3) The ablation product layer weakened the thermal stress-induced mechanical erosion and protected carbon from erosion, which led to the evolution of ablation rates.

## Acknowledgments

The authors are grateful for the financial supports from the National Natural Science Foundation of China (No. 51902239), the Natural Science Foundation of Shaanxi Province, China (No. 2020JQ-808), and the National Innovation and Entrepreneurship Training Program for College Students, China (No. 202110702040).

## References

- [1] ZENG Yi, WANG Di-ni, XIONG Xiang, ZHANG Xun, WITHERS P, SUN Wei, SMITH M, BAI Ming-wen, XIAO Ping. Ablation-resistant carbide Zr<sub>0.8</sub>Ti<sub>0.2</sub>C<sub>0.74</sub>B<sub>0.26</sub> for oxidizing environments up to 3000 °C [J]. *Nature Communications*, 2017, 8: 15836.
- [2] JIA Jian-gang, JU Jia-kang, LIU Shun-wei, JI Gen-shun. Preparation and mechanical properties of C/C composites reinforced with arrayed SiC columnar pins [J]. *Ceramics International*, 2021, 47: 24262–24269.

- [3] FENG Shang-lei, YANG Ying-guo, WANG Jia-min, WANG Yong, ZHOU Xing-tai. Improved mechanical properties and fracture mechanism of C/C composites with salt treatment monitored by synchrotron-based in-situ tensile XRD [J]. *Composites Part B: Engineering*, 2020, 199: 108274.
- [4] KUMAR P, SRIVASTAVA V K. Reciprocating sliding tribology of brake oil treated carbon fiber reinforced ceramic matrix composites [J]. *Transactions of Nonferrous Metals Society of China*, 2019, 29: 1903–1913.
- [5] FANG Hua-chan, XIAO Peng, XIONG Xiang, YU Guang-jun. Microstructures, mechanical and oxidation behaviors of C/C composites modified by NiAl alloy [J]. *Transactions of Nonferrous Metals Society of China*, 2016, 26: 196–202.
- [6] ZHU Yang, ZHANG Qiang, MENG Xiang-li, YAN Lian-sheng, CUI Hong. Adhesive joint properties of advanced carbon/ceramic composite and tungsten-copper alloy for the hybrid rocket nozzle [J]. *International Journal of Adhesion and Adhesives*, 2020, 102: 102670.
- [7] ZHU Xiao-fei, ZHANG Yu-lei, ZHANG Jian, LI Tao, LI Jie, CHEN Rui-cong. A gradient composite coating to protect SiC-coated C/C composites against oxidation at mid and high temperature for long-life service [J]. *Journal of the European Ceramic Society*, 2021, 41: 123–131.
- [8] CHEN Guan-yi, LI Zhuan, XIAO Peng, OUYANG Xi, MA Wen-jie, LI Peng-tao, LI Jin-wei, LI Yang. Tribological properties and thermal-stress analysis of C/C–SiC composites during braking [J]. *Transactions of Nonferrous Metals Society of China*, 2019, 29: 123–131.
- [9] GUO Xia-jun, SI Xiao-qing, LI Chun, ZHAO Shu-hui, LIU Yong-xu, WANG Zhi-quan, HE Zong-jing, WANG Xiao-yang, Cao Jian. Active brazing of C/C composites and single crystal Ni-based superalloy: Interfacial microstructure and formation mechanism [J]. *Journal of Alloys and Compounds*, 2021, 886: 161183.
- [10] LIU Lei, FENG Wei, LI Bo-yan, LI Jian-ping, ZHANG Lei-lei, GUO Yong-chun, HE Zi-bo, CAO Yi, BAO Ai-lin. Particle erosion of C/C–SiC composites with different Al addition in reactive melt infiltrated Si [J]. *Journal of Central South University*, 2020, 27: 2557–2566.
- [11] JORTNER J, PRIYA NS. Applications of carbon/carbon composites [J]. *Comprehensive Composite Materials II*, 2018, 5: 421–435.
- [12] CUI Li-hui, LUO Rui-ying, CUI Guang-yuan. Effect of Al–Mg alloy infiltration on mechanical and electrical properties for carbon/carbon composites [J]. *Crystals*, 2018, 8: 1–18.
- [13] CESCHINI L, MORRI A, BALDUCCI E, CAVINA N, ROJO N, COLOGERO L, POGGIO L. Experimental observations of engine piston damage induced by knocking combustion [J]. *Materials & Design*, 2017, 114: 312–325.
- [14] YIN Jian, ZHANG Hong-bo, XIONG Xiang, TAO Hui-jin, WANG Pei, DENG Chao-yong. Influence of applied load on wear behavior of C/C–Cu composites under electric current [J]. *Progress in Natural Science: Materials International*, 2017, 27: 192–196.
- [15] NIU Yun-song, Xing Ling-ling, YANG Feng, LI Hua-wei, CHEN Ming-hui, ZHU Sheng-long, WANG Fu-hui. Phase structure of sputtered Ta coating and its ablation behavior by laser pulse heating (LPH) [J]. *Journal of Materials Science & Technology*, 2021, 65: 7–17.
- [16] SUN Yang, WANG Yan, LI Yun, ZHOU Ke-chao, ZHANG Lei. Tribological behaviors of Ag–graphite composites reinforced with spherical graphite [J]. *Transactions of Nonferrous Metals Society of China*, 2020, 30: 2177–2187.
- [17] LIU Lei, LI He-jun, FENG Wei, SHI Xiao-hong, WU Heng, ZHU Jun-liang. Effect of surface ablation products on the ablation resistance of C/C–SiC composites under oxyacetylene torch [J]. *Corrosion Science*, 2013, 67: 60–66.
- [18] ZAMAN W, LI Ke-zhi, IKRAM S, LI Wei. Residual compressive and thermophysical properties of 4D carbon/carbon composites after repeated ablation under oxyacetylene flame of 3000 °C [J]. *Transactions of Nonferrous Metals Society of China*, 2013, 23: 1661–1667.
- [19] WANG Shao-long, LI Ke-zhi, LI He-jun, ZHANG Yu-lei, FENG Tao. Structure evolution and ablation behavior of ZrC coating on C/C composites under single and cyclic oxyacetylene torch environment [J]. *Ceramics International*, 2014, 40: 16003–16014.
- [20] REN Jin-cui, ZHANG Yu-lei, ZHANG Peng-fei, LI Tao, LI He-jun, YANG Yang. Ablation resistance of HfC coating reinforced by HfC nanowires in cyclic ablation environment [J]. *Journal of the European Ceramic Society*, 2017, 37: 2759–2768.
- [21] ZHANG Jia-ping, FU Qian-gang, WANG Yong-jie. Interface design and HfC additive to enhance the cyclic ablation performance of SiC coating for carbon/carbon composites from 1750 °C to room temperature under vertical oxyacetylene torch [J]. *Corrosion Science*, 2017, 123: 139–146.
- [22] WANG Chang-cong, LI Ke-zhi, SHI Xiao-hong, HE Qin-chuan, HUO Cai-xia. High-temperature oxidation behavior of plasma-sprayed ZrO<sub>2</sub> modified La–Mo–Si composite coatings [J]. *Materials & Design*, 2017, 128: 20–33.
- [23] KUMAR S, BABLU M, RANJAN A, MANOCHA L M, PRASAD E. Fabrication of 2D C/C–SiC composites using PIP based hybrid process and investigation of mechanical properties degradation under cyclic heating [J]. *Ceramics International*, 2017, 43: 3414–3423.
- [24] LI Pan, JIN Xiao-chao, HOU Cheng, WANG Xiao-bing, YUAN Mei-ni, FAN Xue-ling. Cyclic ablation behaviors of ZrB<sub>2</sub>–SiC composites sintered with nano-sized particles [J]. *Advanced Engineering Materials*, 2018, 20: 1–7.
- [25] ZHANG Jia-ping, FU Qian-gang. The effects of carbon/carbon composites blasting treatment and modifying SiC coatings with SiC/ZrB<sub>2</sub> on their oxidation and cyclic ablation performances [J]. *Corrosion Science*, 2018, 140: 134–142.
- [26] TANG Peng-ju, HU Cheng-long, PANG Sheng-yang, LI Jian, WANG Lei, TANG Su-fang. Interfacial modification and cyclic ablation behaviors of a SiC/ZrB<sub>2</sub>–SiC/SiC triple-layer coating for C/SiC composites at above 2000 °C [J]. *Corrosion Science*, 2020, 169: 108604.
- [27] FENG Guang-hui, LI He-jun, YAO Xi-yuan, HU Dou, YANG Li, LI Bo, LU Jin-hua. Effect of tantalum carbide on the ablation behaviors of hafnium carbide coating for C/C composites under single and cyclic oxyacetylene torch environment [J]. *Surface & Coatings Technology*, 2020, 400: 126219.
- [28] FENG Tao, TONG Ming-de, YAO Shuo-tian, LI He-jun, WEN Shi-feng, LIN Hong-jiao. Effect of free silicon content in inner SiC–Si coating on thermal cyclic ablation behavior and microstructure of ZrC/SiC–Si coating [J]. *Surface & Coatings Technology*, 2020, 393: 125775.
- [29] CHEN Bo-wen, NI De-wei, LU Jun, CAI Fei-yan, ZOU Xue-gang, ZHOU Hai-jun, DONG Shao-ming. Multi-cycle and long-term ablation behavior of C/ZrB<sub>2</sub>–SiC composites at 2500 °C [J]. *Corrosion Science*, 2021, 184: 109385.

- [30] FENG Guang-hui, LI He-jun, YAO Xi-yuan, ZHOU Hang, YU Yu-lan, LU Jin-hua. Ablation resistance of HfC-TaC/HfC-SiC alternate coating for SiC-coated carbon/carbon composites under cyclic ablation [J]. Journal of the European Ceramic Society, 2021, 41: 3207–3218.
- [31] FENG Tao, TONG Ming-de, YAO Shuo-tian, LI He-jun, LIN Hong-jiao, WEN Shi-feng, WANG Pei-pei. Ablation behavior and mechanical property of the B-modified SiC/HfC-SiC composites in cyclic ablation environment [J]. Corrosion Science, 2020, 174: 108829.
- [32] FENG Tao, TONG Ming-de, YAO Shuo-tian, LI He-jun, WEN Shi-feng, LIN Hong-jiao. Effect of PyC interface phase on the cyclic ablation resistance and flexural properties of two-dimensional C<sub>f</sub>/HfC composites [J]. Journal of the European Ceramic Society, 2021, 41: 158–166.
- [33] HU Cheng-long, PANG Sheng-yang, TANG Su-fang, WANG Shi-jun, HUANG Hong-tao, CHENG Hui-ming. Ablation and mechanical behavior of a sandwich-structured composite with an inner layer of C<sub>f</sub>/SiC between two outer layers of C<sub>f</sub>/SiC-ZrB<sub>2</sub>-ZrC [J]. Corrosion Science, 2014, 80: 154–163.
- [34] XIE Jing, LI Ke-zhi, LI He-jun, FU Qian-gang, LIU Lei. Cyclic ablation behavior of C/C-ZrC-SiC composites under oxyacetylene torch [J]. Ceramics International 2014, 40: 5165–5171.
- [35] ZHAO Zhi-gang, LI Ke-zhi, LI Wei, ZHANG Lei-lei. Cyclic ablation behavior of C/C-ZrC-SiC-ZrB<sub>2</sub> composites under oxyacetylene torch with two heat fluxes at the temperature above 2000 °C [J]. Corrosion Science, 2021, 181: 109202.
- [36] LIU Lei, LI Bo-yan, FENG Wei, TANG Cheng-wei, ZHANG Jia-ping, YAO Xi-yuan, YANG Zhong, GUO Yong-chun, WANG Ping, ZHANG Yang. Effect of loading spectrum with different single pulsing time on the cyclic ablation of C/C-SiC-ZrB<sub>2</sub>-ZrC composites in plasma [J]. Corrosion Science, 2021, 192: 109817.
- [37] SUN Wei, HAO Zhen-hua, XIONG Xiang, XU Yong-long. Microstructure and cyclic ablation behaviour of a Si-Mo-Ti protected C/C composites by a two-step method [J]. Materials at High Temperatures, 2021, 38: 114–122.
- [38] TATARKO P, VALENZA F, UNSAL H, KOVALCIKOVA A, SEDLACEK J, SAJGALIK P. Design of Lu<sub>2</sub>O<sub>3</sub>-reinforced C<sub>f</sub>/SiC-ZrB<sub>2</sub>-ZrC ultra-high temperature ceramic matrix composites: Wetting and interfacial reactivity by ZrSi<sub>2</sub> based alloys [J]. Journal of the European Ceramic Society, 2021, 41: 3051–3060.
- [39] JIA Yan, CHEN Si-an, LI Yong, WANG Song, HU Hai-feng. High-temperature mechanical properties and microstructure of C/C-ZrC-SiC-ZrB<sub>2</sub> composites prepared by a joint process of precursor infiltration and pyrolysis and slurry infiltration [J]. Journal of Alloys and Compounds, 2019, 811: 151953.
- [40] RAN Li-ping, RAO Fei, PENG Ke, YIN Huan, YI Mao-zhong. Preparation and properties of C/C-ZrB<sub>2</sub>-SiC composites by high-solid-loading slurry impregnation and polymer infiltration and pyrolysis (PIP) [J]. Transactions of Nonferrous Metals Society of China, 2019, 29: 2141–2150.
- [41] LI He-jun, YAO Xi-yuan, ZHANG Yu-lei, LI Ke-zhi, GUO Ling-jun, LIU Lei. Effect of heat flux on ablation behavior and mechanism of C/C-ZrB<sub>2</sub>-SiC composite under oxyacetylene torch flame [J]. Corrosion Science, 2013, 74: 265–270.
- [42] LIU Lei, LI He-jun, ZHANG Yu-dan, SHI Xiao-hong, FU Qian-gang, FENG Wei, FENG Tao. Effect of ZrB<sub>2</sub> and SiC distributions on the ablation of modified carbon/carbon composites [J]. Ceramics International, 2015, 41: 1823–1829.
- [43] CHEN Bo-wen, NI De-wei, LIAO Chun-jing, JIANG You-lin, LU Jun, DONG Shao-ming. Long-term ablation behavior and mechanisms of 2D-C<sub>f</sub>/ZrB<sub>2</sub>-SiC composites at temperatures up to 2400 °C [J]. Corrosion Science, 2020, 177: 108967.
- [44] WANG Peng, LI Su-juan, WEI Chun-cheng, HAN Wen-bo, WEN Guang-wu, GENG Xin, LI Shuang, SUN Hai-bin, LI Xiao-wei. Microstructure and ablation properties of SiC/ZrB<sub>2</sub>-SiC/ZrB<sub>2</sub>/SiC multilayer coating on graphite [J]. Journal of Alloys and Compounds, 2019, 781: 26–36.

## C/C-SiC-ZrB<sub>2</sub>-ZrC 复合材料 在等离子体高频脉冲达 2000 次过程中的烧蚀特性

冯薇<sup>1</sup>, 张妍<sup>1</sup>, 刘磊<sup>1</sup>, 李博岩<sup>1</sup>, 张佳平<sup>2</sup>, 陈曦<sup>3</sup>, 何子博<sup>1</sup>, 唐成伟<sup>1</sup>, 张海军<sup>1</sup>, 韩秦鑫<sup>1</sup>

1. 西安工业大学 材料与化工学院, 西安 710021;
2. 西北工业大学 凝固技术国家重点实验室, 西安 710072;
3. 西安稀有金属材料研究院有限公司, 西安 710072

**摘要:** 研究等离子体单次毫秒级加载条件下 C/C-SiC-ZrB<sub>2</sub>-ZrC 复合材料在不同次数高频脉冲过程中的烧蚀行为与机理。烧蚀试验在自研台架上进行, 测试过程中等离子体-空气射流交替冲击试样表面。结果表明, 随冲击次数增加, 前 1000 次内烧蚀率迅速下降, 随后在达 2000 次过程中烧蚀率缓慢降低。微结构、物相及烧蚀表面温度特征说明烧蚀试样表面形成一层不完整的混合陶瓷烧蚀产物层, 且裸露的碳含量在 1000 次冲击烧蚀以后趋于稳定。烧蚀产物层削弱了热应力诱发的机械剥蚀并保护其亚层的碳不被侵蚀, 进而导致烧蚀率的演变。

**关键词:** 往复烧蚀; 脉冲烧蚀; C/C 复合材料; SiC-ZrB<sub>2</sub>-ZrC; 循环次数

(Edited by Bing YANG)